Iranian Journal of Medical Physics
Vol. 9, No. 4, Autumn 2012, 253-263
Received: July 18, 2012; Accepted: December 16, 2012

Original Article

Preliminary Results of Treating Cancerous Cells of Lung (QU-DB) by Hyperthermia using Diode Laser and Gold Coated Fe_3O_4/SiO_2 Nano-Shells: An in-Vitro Assay

Mohammad Etrati Khosroshahi[1,2*], Lida Ghazanfari[1], Zahra Hasan-Nejad[1]

Abstract

Introduction
In this study, we describe the results of controlled synthesis and application of gold coated Fe_3O_4/SiO_2 nano-shells combined with the optical property of gold for enhancement of selective photothermal interaction with cancerous cells based on the surface plasmon resonance (SPR) Phenomena.

Materials and Methods
Magnetite Nano-Particles (MNPs) were prepared by means of co-precipitation. MNPs were modified with a thin layer of Silica using the Stober method. The amino-modified Fe_3O_4/SiO_2 nano-shells were covered with gold colloids as a self-assembeled process. In-vitro assays were performed to determine the effect of apoptosis of the cells based on the cells morphological changes.

Results
The biologically inert nano-shells (85 nm) with a Magnetite/Silica core and a gold shell were optically activated. A successful laser-hyperthermia based on the thermal effect of surface plasmon resonance was performed using different gold concentrations. The thermal profile effects of laser power are presented as ideal cases of nanoshell-assisted photo-thermal therapy. The thermally-induced cell death has been shown to be dependent on NPs concentration and laser power density. The power densities of 157 and 184 W/cm^2 caused complete cell death at the focal point of the laser beam. Cell damage was reduced by decreasing the power density of laser. Also, a larger area of damage on cell culture plates was observed at longer intervals of laser irradiation.

Conclusion
An optimized laser-(SPR) hyperthermia was obtained using a concentration of gold coated Fe_3O_4/SiO_2 nano-shells concentration=0.1 mg/ml at intensity=157 W/cm^2 at 60s.

Keywords: Diode Laser, Hyperthermia, Lung Cancerous Cell, Metallic Nano-Shells, Surface Plasmon Resonance

1-Laser and Nano-biophotonics Lab., Biomaterial Group, Faculty of Biomedical Engineering, Amirkabir University of Technology, Tehran, Iran.
2- Laser, optics and photonics research center, Tehran, Iran.
*Corresponding author: Tel: +98 2164542398. Fax: +98 21 66468186. Email: khosro@aut.ac.ir

1. Introduction

The increasing availability of nano-structures with highly controlled magnetic and optical properties in the nano-meter size range has created widespread interest in the use of Nano-Particles (NPs) for the diagnosis and treatment of cancer [1]. As early as the late 1800s, physicians were using heat as treatment for cancer [2]. Generally, temperatures above 42 °C can induce cell death in some tissues in the range of 41 °C - 47 °C beginning to show signs of apoptosis [3-5]. Local hyperthermia of 43 °C during chemotherapy infusion produces a "more than additive" increase in cell death compared to chemotherapy alone [6]. Clinically, several types of cancer had complete increased response rates by an absolute 16%-26% when hyperthermia was added to standard external beam radiotherapy [7]. A form of non-ionizing radiation, micro-wave coagulation therapy induces necrosis by hyperthermia in an invasive fashion similar to Radio Frequency Ablation (RFA) [8]. In an attempt to minimize the risks of generalized hyperthermia, various non-invasive techniques such as nano-particle hyperthermia technology is intended to be used as an adjuvant to radiation therapy [9-11].

Metal nano-particles exemplify the potential for application in targeted hyperthermic therapy. In recent decades, magnetic NPs, especially Fe_3O_4 (Magnetite) and γ-Fe_2O_3 (Maghemite), have attracted increasing interest, because of their outstanding properties including super-para-magnetism, and low toxicity, and, as a result, their potential applications in various fields, especially in hyperthermia, enzyme-immobilization, bio-sensing and bio-electro-catalysis, separation and purification [12-16]. Various approaches have been explored for synthesis of high-quality magnetic Iron-oxide NPs [17-22]. There have been extensive reports on the synthesis of magnetic core/shell nano-particles in which the core is Fe_3O_4 and the shell consists of a metal or metal-oxide. In recent years, much effort has been devoted to the synthesis and characterization of Silica (SiO_2)-coated Iron-oxide NPs [23-29].

The advantage of the gold nano-shells compared to the Iron-oxide nano-particles is the possibility of engineering them with optical properties suitable for combined imaging and therapy [30,31]. On the other hand, the advantage of magnetic nano-particles is that their movement can be controlled with an external magnetic field so that they can be immobilized close to the targeted tissue [32]. Furthermore, they can be used in magnetic resonance imaging (MRI), due to their high transverse relaxitivity [33,34]. However, when Silica and gold are added, the magnetization saturation values of the resultant nano-composite will be decreased.

Due to the high dielectric constant of Silica, the three-layered $Fe_3O_4/SiO_2/Au$ nano-composite would be a stronger light- absorber than the two-layered gold nano-shell [35, 36]. Localized surface plasmon resonance (LSPR), simply defined as collective oscillations of conductive electrons in the metal nano-particles [37]. By a well designed structure including the shape and size of the nano-shell i.e. core-shell ratio, one can expect, based on the Mie theory, to achieve a tunable nano system ranging from visible to near infrared (NIR) [38, 39]. Specifically, this procedure can be used to produce hyperthermia in malignant tumors with the goal of locally inducing cellular necrosis or weakening tumorous tissue into a state where necrosis can occur using a lower than required dose of ionizing radiation from radiation therapy [40]. We know that the small particles in the 60–400 nm size range will extravagate and accumulate in tumors [41,42] via a passive mechanism referred to as the 'enhanced permeability and retention' (EPR) effect [43]. The particles accumulate passively, then generate heat upon laser light illumination [44,45].

We currently used gold nano-shells for wound healing purposes [46]. Here, we first synthesize the gold- coated Fe_3O_4/SiO_2 nano-shells, and then describe the use of these absorbing nano-shells in NIR heat generation. The principle goal of this report is to determine the efficacy of these three-layered

nano-shells in laser-hyperthermia of cancerous lung cells.

2. Materials and Methods

2.1. Synthesis and coating of Fe_3O_4/SiO_2 nano-shells with gold

Fe_3O_4-NPs and SiO_2-coated Fe_3O_4-NPs were synthesized by means of chemical co-precipitation and Stober methods [47]. To coat the Fe_3O_4/SiO_2 nano particles with gold the following steps were taken: 65 µl of 3 amino propyl triethoxy silane (APTS- Sigma-Aldrich) was added to a 200 ml of the MNP solution, and the mixture was vigorously stirred for 2h and refluxed. Then, to a 45 ml Aliquot of milli-Q water (specific conductance 0.1 µS/cm- deoxygenated by bubbling N_2 gas for 1h prior to the use) 0.5 ml of 1 M NaOH (Merck) and 1 ml of tetrakis (hydroxymethyl) phosphonium chloride (THPC- Sigma-Aldrich) solution was added [48]. The mixture was vigorously stirred for 5 minutes. Then, 2 ml of 1% Chloro-Auric acid ($HAuCl_4$- Sigma-Aldrich) in water was added quickly to the stirred solution. After that an aliquot of APTS-functionalized Silica-NPs dispersed in 1ml of Ethanol (Merck) was placed in a centrifuge tube along with an excess of gold- NPs (5 ml of gold colloid solution). Finally, 25 mg of Potassium Carbonate (K_2CO_3- Sigma-Aldrich) was dissolved in 100 ml of water and after 10 minutes of stirring, 1.5 ml of 1% $HAuCl_4$ was added. 200 µl of the solution containing the Fe_3O_4/SiO_2/Au nano-composites was added to 4 ml of the colorless solution. The gold nano-shells were prepared by reduction of the gold solution with Formaldehyde (37%- Sigma-Aldrich). After 2-4 minutes, the solution changed color to dark pink, which is characteristic of nano-shell formation.

2.2. Preparation of cells and gold-coated Fe_3O_4/SiO_2 nano-shell compounds

QU-DB lung cancer cells (purchased from the Pasteur Institute, National Cell Bank of Iran) were seeded in 96-well tissue culture plates and incubated at 37ºC and 5% CO_2. Dulbecco's Modified Eagle Medium (DMEM-GIBCO) supplemented with 10% fetal bovine serum (FBS- GIBCO) was used as cell culture medium (C.C.M.). The serum-free cell culture medium containing nano-particles was placed under UV for 4 hours before being added to cell cultures. After a 24 hour incubation period, cell culture medium was replaced with two different concentrations of gold nano-shell suspensions including 0.01 and 0.1 mg/ml. The nano-shells used in our experiments had a diameter of ~85 nm (75-100nm) and an average shell thickness of ~35 nm which was measured with transmission electron microscopy (TEM) and particle size distribution of gold coated Fe_3O_4/SiO_2 nano-shells as shown in Figures 1a,b. TEM imaging shows clusters of small gold NPs assembled on the surface of larger Silica NPs. The self-assembled aggregates consist of tens of gold NPs.

AFM images of nano-shells shown in figure 1c are expected to show a considerable surface roughness due to the agglomeration of the nano-shells. In our case, negative skewness or measure of symmetry over the surface profile indicates the predominance of valleys.

As shown in figure 2, the optical absorption spectrum range of Fe_3O_4/SiO_2/Au nano-structures is relatively broad compared with that of pure gold colloid. In addition, the plasmon line-width is dominated by electron surface scattering. According to Mie's theory [49], the broadening of resonance absorption is related to the size, shape, and aggregation of the gold nano-shells.

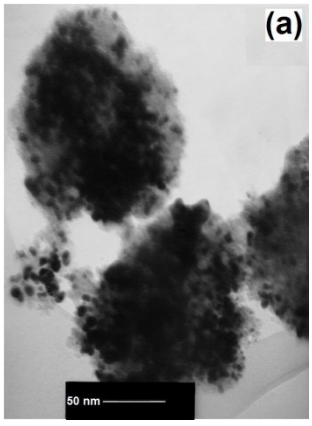

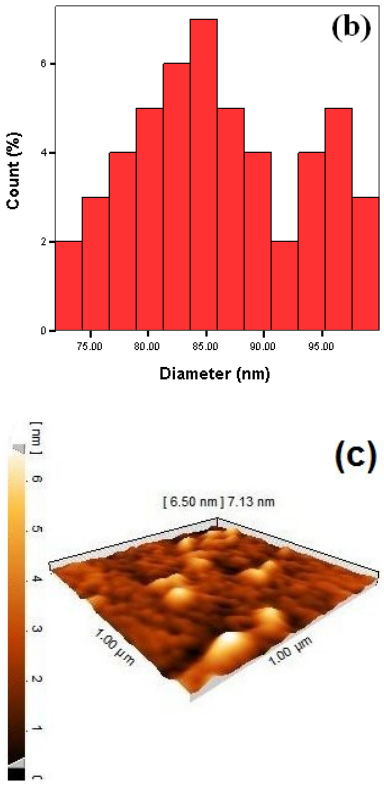

Figure 1. (a) TEM image, (b) particle size distribution, and (c) AFM micrographs in 3D-height mode of gold coated Fe_3O_4/SiO_2 nano-shells

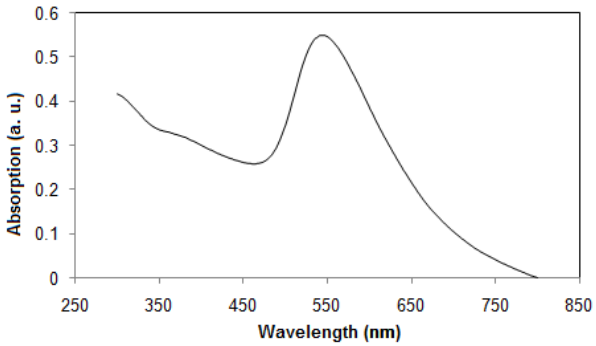

Figure 2. UV-vis spectra of $Fe_3O_4/SiO_2/Au$ nanostructures

2.3. In-vitro assay

In in-vitro assay the cell-NP medium was irradiated by a home-made NIR diode laser at 800 nm ± 10 nm with a focal spot of 7 mm^2. Cells were divided into two groups. The first group was exposed to nano-shells and NIR-laser, and the second one was irradiated by NIR-laser alone. The effect of hyperthermic treatment and heat-induced apoptosis was evaluated according to alteration of cell morphology. Live QU-DB lung cancer cells have a fibroblast-like morphology while damaged cells shrink and have a rounded shape [50]. The temperature was monitored by a digital thermometer with 0.1 °C precision (CHY502A1, MULTI LOGGER) connected to a laptop for further processing. The thermometer was cleaned with warm, soapy water, and then wipes were used for anti-bacterial sterilization.

The main advantage of using NIR lasers with for laser-hyperthermia is their relatively deep penetration due to low absorption coefficients (0.02 to 0.30 cm^{-1}) of haemoglobin, melanin, and water in the region between 650 and 900 nm [51]. Penetration depths of several centimeters have been reported for breast and brain tissues [41,52].

3. Results

The temperature change of the two DMEM groups containing nano-shells with different concentrations of 0.01 and 0.1 mg/ml were studied at 184 W/cm^2 for a period of 3 minutes. Also, one group was irradiated without NPs as a control group (figure 3a). A maximum temperature rise of 6°C was achieved at 184 W/cm^2 in the control group where it remained constant for the rest of the irradiation time. The temperature reached 44 - 48°C at 184 W/cm^2 after 20 seconds at concentrations of 0.01 and 0.1 mg/ml, respectively. A temperature change of 8°C was observed after 40 seconds between 14-184 W/cm^2 for a concentration of 0.1 mg/ml and on further heating it reached 59°C after 100 seconds (i.e. 22 °C rise). In comparison, no significant temperature change was observed when pure cell culture medium was exposed to the laser light. Similarly, the experiment was repeated when QU-DB lung cancerous cells were added to the (DMEM-NP) medium for 0.01 mg/ml (figure 3b) and 0.1 mg/ml (Figure 3c). These experiments were repeated three times to confirm the reproducibility of the data.

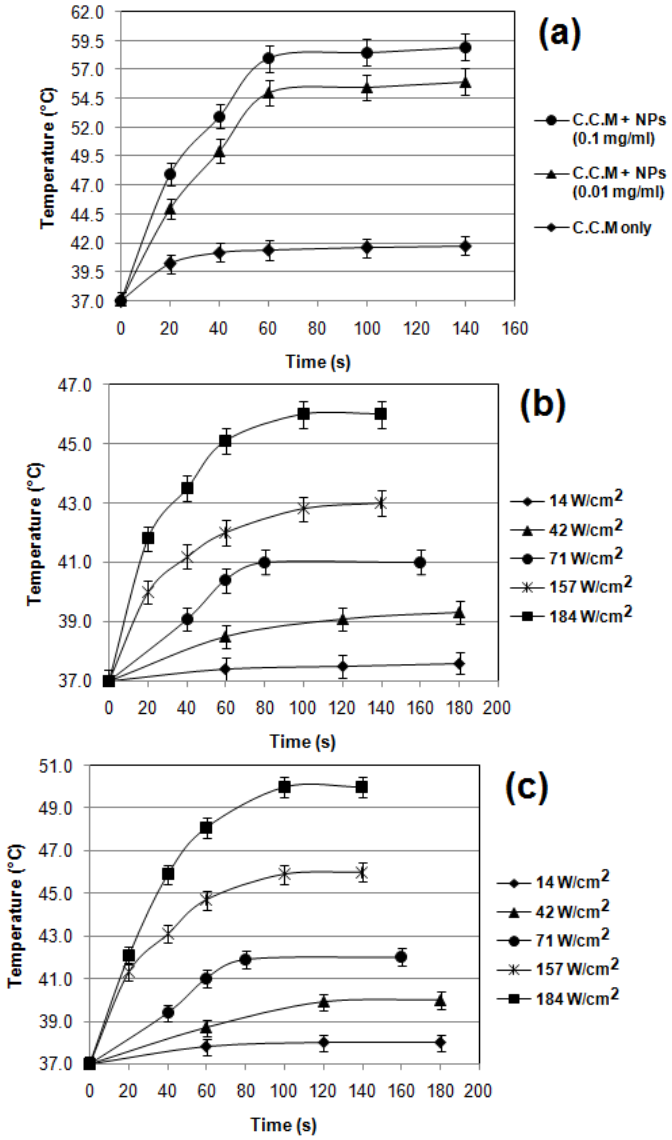

Figure 3. Temperature change (ΔT) over a period of 3 minutes (a) at maximum laser power density of 184 W/cm^2 for C.C.M. only and C.C.M. + MNPs at different concentrations of 0.01 and 0.1 mg/ml, (b) at various laser power densities for C.C.M. + MNPs at concentration of 0.01 mg/ml + QU-DB lung cancer cells, (c) at various laser power densities for C.C.M. + MNPs at concentration of 0.1 mg/ml + QU-DB lung cancer cells

Irradiation of combined NPs, DMEM and QU-DB lung cancer cells showed that the temperature increased with increased exposure time.

This study was performed under two different conditions. Sever hyperthermic treatment within a short time and mild hyperthermic treatment over a long time. In the first group, cells are irradiated with 184, 157, and 71 W/cm^2 for a minute and the second group with 42 and 14 W/cm^2 for 3 minutes. The example of cancer cells, treatment before and after laser-hyperthermia at different power densities are showed in figure 4. Normal morphology of cancer cells i.e. before treatment is depicted in figure 4a. Initially, to determine the effect of laser on cultured cells without nano-particles, they were irradiated at 184 W/cm^2 and as is shown in figure 4b there is no significant change in cell morphology.

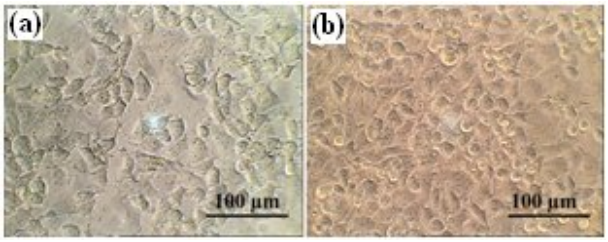

Figure 4. Optical microscopy of (a) control cells (untreated tumoric cells) 24 hours after subculture and (b) the cells after laser treatment without nano-shells

Figure 5 demonstrates the cellular morphology changes at 184, 157, and 71 W/cm^2 for one minute. As illustrated in Figure 6, by increasing the treatment time to 180 seconds at 14 and 42 W/cm^2, the damaged area is extended, and more cells at the region far from the laser beam are affected because of heat transfer. Nevertheless, by decreasing the power density, a more limited damage area was observed for the same exposure time.

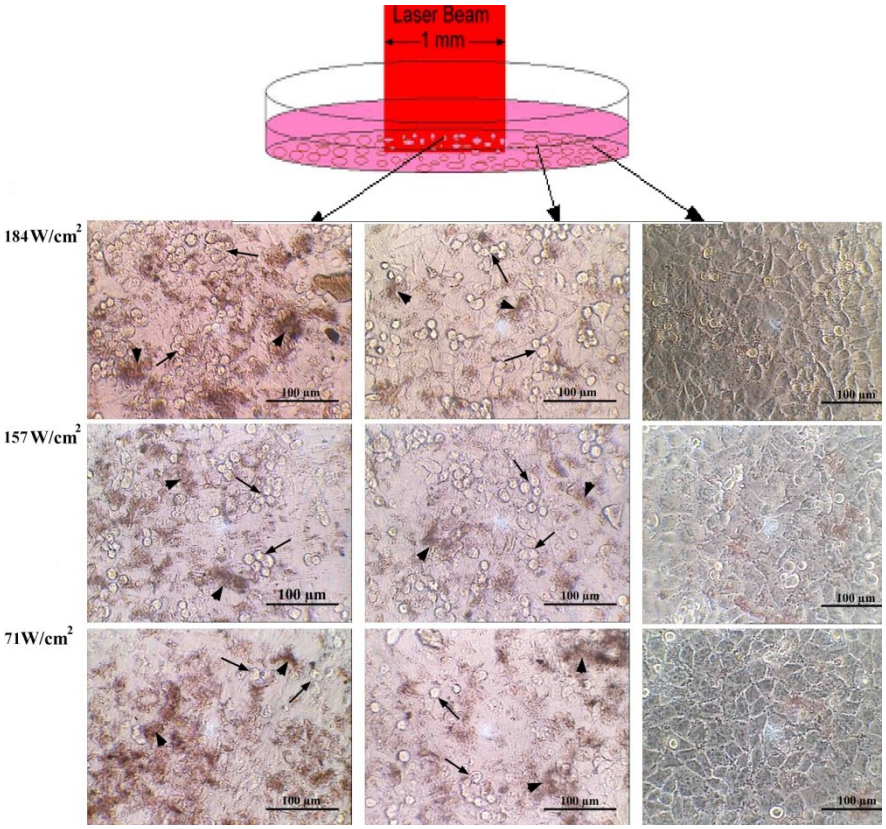

Figure 5. Illustration of QU-DB lung cancer cells after laser irradiation at 71, 157 and 184 W/cm^2 and 0.1mg/ml for 60 s. Three different regions were photographed and depicted in a row: the focal point of the laser beam at the center (left), the adjacent region (middle) and far region (right). Arrow head: nano-shells colonies; arrow: dead cells

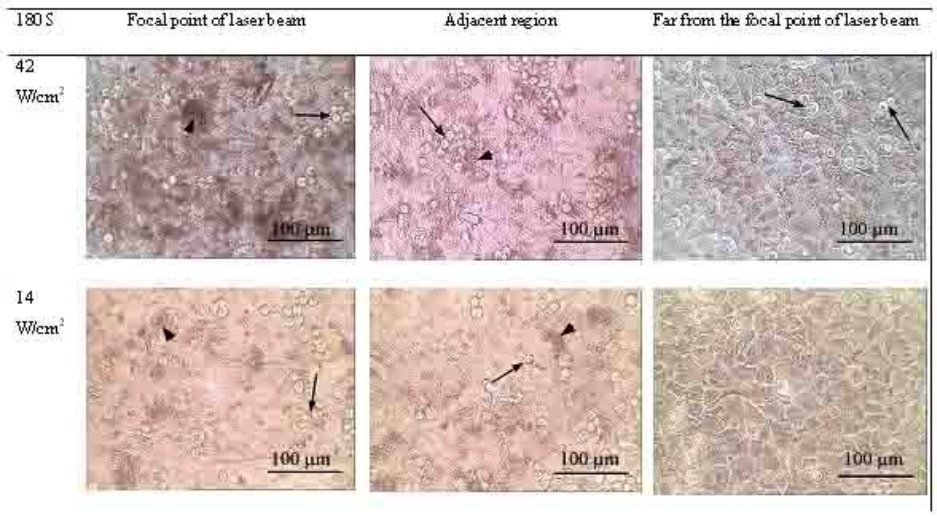

Figure 6. Illustration of QU-DB lung cancer cells after laser irradiation at different powers of 14 and 42 W/cm^2 and 0.1mg/ml for 180 s. Three different parts were photographed and depicted in a row: the focal point of the laser beam at the center (left), the adjacent region (middle) and far region (right). Arrow head: nano-shells colonies; arrow: dead cells

The effect of NPs, concentration on cell apoptosis is shown in figure 7 where the proportion of damaged cells is reduced by decreasing the concentration to 0.01 mg/ml at 157 W/cm^2 during a one minute exposure.

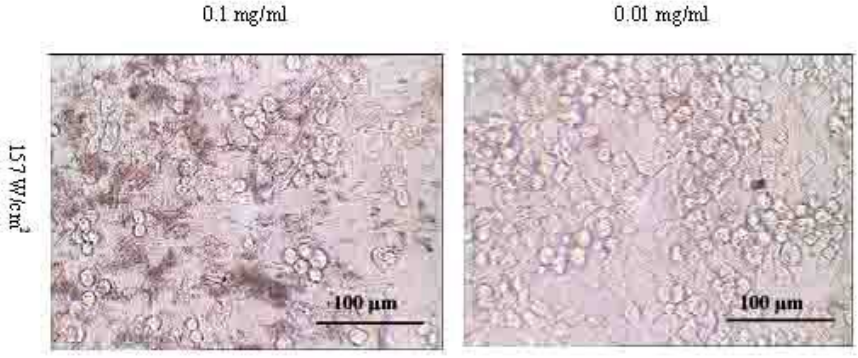

Figure 7. Illustration of QU-DB lung cancer cells after hyperthermia treatment at two different concentrations of gold coated Fe_3O_4/SiO_2 nano-shells: 0.1 mg/ml (left) and 0.01 mg/ml (right) at 60s. More colonies and apoptotic cells can be seen in the sample with concentration of 0.1 mg/ml

4. Discussion

Nano-particles' plasmon resonance is sensitive to changes of their dielectric microenvironment [53]. In contrast to irradiated gold coated Fe_3O_4/SiO_2 nano-shells dispersed in the DMEM, the concentration of nano-shells has significant effects on the amount of heat generated at a given power density. For core–shell, the NP efficiency parameter has the form [54]

$$\frac{\Delta T_0}{I_0} = \frac{K_{abs} r_1}{4k_\infty} \times \left[1 - \exp\left(- \frac{3k_\infty t_p}{r_1^2 (c_0 \rho_0 r_0^3 + c_1 \rho_1 (1 - r_0^3 / r_1^3))} \right) \right] \quad (1)$$

where I_0 is constant and equal to the intensity of the laser radiation during pulse duration t_p, K_{abs} is the efficiency factor of absorption, k_∞ is the coefficient of thermal conduction of the ambient medium, c_0, ρ_0 and c_1, ρ_1 are the heat capacity and density of the material of the core (Magnetite-Silica) and shell (Gold) accordingly, r_0 and r_1 are the radii of the core and shell and the thickness of the shell $r_0 = r_1 - r_0$. Maximum value of the parameter $\Delta T_0/I_0$ indicates the efficiency of transformation of absorbed optical energy by NPs into thermal energy. In our case this corresponds to about 12% and 7% for C.C.M. + MNPs at a concentration of 0.1 mg/ml and C.C.M. + MNPs at a concentration of 0.01 mg/ml + QU-DB lung cancer cells, respectively.

The effect of hyperthermic treatment and heat-induced apoptosis was evaluated according to alteration of cell morphology. Cell membrane, cytoskeleton [42], intracellular proteins[55], nucleic acid and mitochondrial function [56] are molecular effectors during hyperthermia. Studies have shown the shrinkage of endothelial cells in response to heat stress [42]. The shrinking or morphological changes have been attributed to diseggregation of the cytoskeleton after hyperthermia [42]. This phenomenon has been supported in electron microscopic studies [57]. Actin filaments become insoluble during hyperthermia [56]. Changes in cell membrane function were considered as the main cause of cell death. Observation of altered membrane fluidity, permeability and surface blebbing with increase in temperature, support this concept [56]. These phenomena may become evident during the recovery phase of the cell to the base-line temperature, but not immediately after heating [57]. Cells undergoing apoptosis shrink and exhibit cytoplasmic and chromatin condensation. In the final stages, cells become fragmented into small apoptotic bodies [58].

The induction of cell death has been shown to involve concentration and power depending on the gold -coated Fe_3O_4/SiO_2 nano-shells and the applied laser. The results indicate that these nano-shells acted as an efficient photo-thermal mediator. By increasing the power density, the temperature rise became faster and higher. One important aspect of this finding was that the maximum temperature of 56 and 59°C of C.C.M fell to ≈ 46 and 50°C for 0.01 mg/ml and 0.1 mg/ml, respectively which can be attributed to the protein adsorption in the presence of cells. Optical microscopy showed

that the majority of cells became circular due to thermal stress. It is clearly apparent in optical microscopic pictures that most of the gold-coated Fe_3O_4/SiO_2 nano-shells accumulated in the center of the wells, where the laser beam was focused. This may be due to the movement of gold -coated Fe_3O_4/SiO_2 nano-shells in the direction of the gradient force towards the center of the beam [59].

As shown in Figure 6, all of the cells in the region of irradiation have a circular shape which is the characteristic of apoptotic cells [50]. The percentage of apoptosis was calculated by dividing the total number of rounded cells by the total number of cells at the focal point of the laser as well as the immediate surrounding area (6×10^4 μm^2). As shown in Figure 8, at 184 and 157 W/cm^2 and irradiation time of 60 s all of the cells suffered apoptosis. But, the heat-inducted death was reduced to 92.78% at lower power density (71 W/cm^2) at the same period of time. The percentage of damaged cells and gold nano-shells decreases with the increase of distance from the center of the beam. Likewise, treatment was carried out at a lower energy and a longer time. In this situation, the percentage of damaged cells was reduced to 57% and 47.15% at 42 and 14 W/cm^2, respectively. But, as illustrated in Figure 6, the area of damaged cells is extended because of heat transfer. This experiment was repeated three times in order to prove the observed reproducibility of the data.

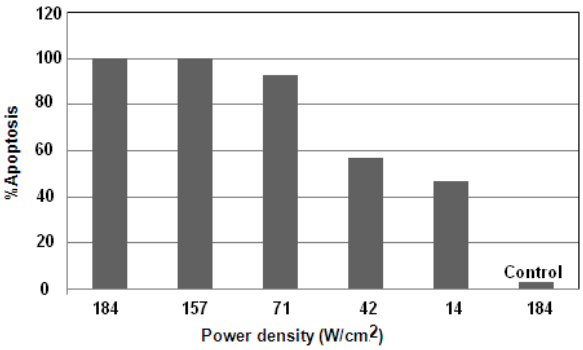

Figure 8. The effect of laser energy on heat-induced apoptosis for C.C.M. + MNPs at concentration of 0.1 mg/ml + QU-DB lung cancer cells at 60s. Control group stands for laser irradiated QU-DB lung cancer cells without MNPs

Our results indicate that laser power density is one of the important parameters during laser-hyperthermia which affects the extent of cell death. Also, the results showed that apoptosis of cells increased by increasing the laser power density in both concentrations of nano-shells, which effectively implies that temperature and its variations play a crucial role in the laser-hyperthermia process.

In the thermal damage process, the endpoint damage Ω inside the irradiated tissue can be estimated by solving the Arrhenius integral [60], assuming that damage is due to thermal denaturation of proteins. Hence,

$$\Omega(t) = \ln\left[\frac{C_0}{C_t}\right] \qquad (2)$$

Where C_0 is the initial concentration of the native state (undamaged) tissue constituent molecules, C_t is the concentration of undamaged molecules after time (t). Conventionally, Ω(t)=0 implies no tissue damage at all, Ω(t)=1 means that most (i.e. 63%) of the tissue is damaged and Ω(t)>1 indicates a complete irreversible damage. Based on our results, Ω(t)>1 for cancer cells at 157, 184 W/cm^2 for 60s using NPs concentrations of 0.1mg/ml.

What the preferred cell temperature should be, at least during an in-vitro operation, remain controversial, varying along the above parameters with apposition pressure, cell type and chemical composition and the likely age of the cell which requires further investigation. All in all, in our experiment an optimized laser hyperthermia condition was obtained by using a high concentration of gold nano-shells concentration=0.1 mg/ml, intensity=157W/cm^2 at 60s.

5. Conclusion

In conclusion, gold shells were formed on the surfaces of Fe_3O_4/SiO_2 nano-shells. Mono-disperse Fe_3O_4/SiO_2 core–shell spheres with a size of about 50 nm can be prepared using the Stober method by first modifying outer Silica shells terminated with Silanol groups. Fe_3O_4/SiO_2 spheres were then served as the

hosts and gold NPs were assembled on their surfaces by electrostatic interaction in order to form gold-coated Fe_3O_4/SiO_2 nano-shells. The prepared particles are relatively uniform in size. Two nano-shell concentrations (0.01 and 0.1 mg/ml), at different power densities, were tested where the irradiation process was simulated using one diode laser. The efficiency of the transformation of absorbed optical energy by NPs into thermal energy was about 12% and 7% for C.C.M. + MNPs at a concentration of 0.1 mg/ml and C.C.M. + MNPs at a concentration of 0.01 mg/ml + QU-DB lung cancer cells, respectively. Based on the SPR-induced thermal effect and Mie's theory, higher concentrations of gold nano-particles produce a higher temperature rise. The 100% cell damage was achieved at 157 W/cm^2 using 0.1 mg/ml nano-shells. The maximum temperature measured of cells with cell culture medium was about 59°C at 184 W/cm^2, using 0.1 mg/ml nano-shells. The preliminary results demonstrate that the application of gold nano-shells together with NIR laser is possible based on the SPR mechanism, provided an operating condition including the power density and NPs, concentration is clearly optimized.

References

1. Hartman KB, Wilson LJ, Rosenblum MG. Detecting and treating cancer with nanotechnology. Mol Diagn Ther. 2008;12(1):1-14.
2. Field SB, Bleehen NM. Hyperthermia in the treatment of cancer. Cancer Treat Rev. 1979 Jun;6(2):63-94.
3. Milleron RS, Bratton SB. 'Heated' debates in apoptosis. Cell Mol Life Sci. 2007 Sep;64(18):2329-33.
4. Hildebrandt B, Wust P, Ahlers O, Dieing A, Sreenivasa G, Kerner T, et al. The cellular and molecular basis of hyperthermia. Crit Rev Oncol Hematol. 2002 Jul;43(1):33-56.
5. Lee H, Kim S, Choi BH, Park MT, Lee J, Jeong SY, et al. Hyperthermia improves therapeutic efficacy of doxorubicin carried by mesoporous silica nanocontainers in human lung cancer cells. Int J Hyperthermia. 2011;27(7):698-707.
6. Issels RD. Hyperthermia adds to chemotherapy. Eur J Cancer. 2008 Nov;44(17):2546-54.
7. Van Der Zee J, Gonzalez Gonzalez D, Van Rhoon GC, Van Dijk JD, Van Putten WL, Hart AA. Comparison of radiotherapy alone with radiotherapy plus hyperthermia in locally advanced pelvic tumours: a prospective, randomised, multicentre trial. Dutch Deep Hyperthermia Group. Lancet. 2000 Apr 1;355(9210):1119-25.
8. Curley SA. Radiofrequency ablation of malignant liver tumors. Oncologist. 2001;6(1):14-23.
9. Curley SA, Cherukuri P, Briggs K, Patra CR, Upton M, Dolson E, et al. Noninvasive radiofrequency field-induced hyperthermic cytotoxicity in human cancer cells using cetuximab-targeted gold nanoparticles. J Exp Ther Oncol. 2008;7(4):313-26.
10. Kalambur VS, Longmire EK, Bischof JC. Cellular level loading and heating of superparamagnetic iron oxide nanoparticles. Langmuir. 2007 Nov 20;23(24):12329-36.
11. Cherukuri P, Glazer ES, Curley SA. Targeted hyperthermia using metal nanoparticles. Adv Drug Deliv Rev. 2010 Mar 8;62(3):339-45.
12. Bouzier-Sore AK, Ribot E, Bouchaud V, Miraux S, Duguet E, Mornet S, et al. Nanoparticle phagocytosis and cellular stress: involvement in cellular imaging and in gene therapy against glioma. NMR Biomed. 2010 Jan;23(1):88-96.
13. Jordan A, Scholz R, Wust P, Fähling H, Roland F. Magnetic fluid hyperthermia (MFH): Cancer treatment with AC magnetic field induced excitation of biocompatible superparamagnetic nanoparticles. Journal of Magnetism and Magnetic Materials. 1999;201(1–3):413-9.
14. Pedro T, María del Puerto M, Sabino V-V, Teresita G-C, Carlos JS. The preparation of magnetic nanoparticles for applications in biomedicine. Journal of Physics D: Applied Physics. 2003;36(13):R182.
15. Corot C, Robert P, Idee JM, Port M. Recent advances in iron oxide nanocrystal technology for medical imaging. Adv Drug Deliv Rev. 2006 Dec 1;58(14):1471-504.
16. McCarthy JR, Weissleder R. Multifunctional magnetic nanoparticles for targeted imaging and therapy. Adv Drug Deliv Rev. 2008 Aug 17;60(11):1241-51.
17. Chertok B, David AE, Moffat BA, Yang VC. Substantiating in vivo magnetic brain tumor targeting of cationic iron oxide nanocarriers via adsorptive surface masking. Biomaterials. 2009 Dec;30(35):6780-7.
18. Zhang J, Post M, Veres T, Jakubek ZJ, Guan J, Wang D, et al. Laser-assisted synthesis of superparamagnetic Fe@Au core-shell nanoparticles. J Phys Chem B. 2006 Apr 13;110(14):7122-8.

19. Liu XM, Fu SY, Xiao HM. Fabrication of octahedral magnetite microcrystals. Materials letters. 2006;60(24):2979-83.
20. Wan J, Yao Y, Tang G. Controlled-synthesis, characterization, and magnetic properties of Fe3O4 nanostructures. Applied Physics A: Materials Science & Processing. 2007;89(2):529-32.
21. Ghasemi E, Mirhabibi A, Edrissi M. Synthesis and rheological properties of an iron oxide ferrofluid. J Magn Magn Mater. 2008;320(21):2635-9.
22. Khosroshahi ME, Ghazanfari L. Comparison of magnetic and rheological behaviour of uncoated and PVA-coated Fe3O4 nanoparticles synthesized under N2 gas. J Magn Magn Mater 2012;324:4143-6.
23. Alcalá M, Real C. Synthesis based on the wet impregnation method and characterization of iron and iron oxide-silica nanocomposites. Solid State Ionics. 2006;177(9):955-60.
24. Stjerndahl M, Andersson M, Hall HE, Pajerowski DM, Meisel MW, Duran RS. Superparamagnetic Fe3O4/SiO2 nanocomposites: enabling the tuning of both the iron oxide load and the size of the nanoparticles. Langmuir. 2008 Apr 1;24(7):3532-6.
25. Kobayashi Y, Saeki S, Yoshida M, Nagao D, Konno M. Synthesis of spherical submicron-sized magnetite/silica nanocomposite particles. J Sol-Gel Sci Tech. 2008;45(1):35-41.
26. Yang D, Hu J, Fu S. Controlled Synthesis of Magnetite− Silica Nanocomposites via a Seeded Sol− Gel Approach. J Phys Chem C. 2009;113(18):7646-5
27. Khosroshahi ME, Ghazanfari L, Tahriri M. Characterisation of binary (Fe3O4/SiO2) biocompatible nanocomposites as magnetic fluid. J Exp Nanosci. 2011;6(6):580-95.
28. Khosroshahi ME, Ghazanfari L. Amino surface modification of Fe3O4/SiO2 nanoparticles for bioengineering applications. Surface Engineering. 2011;27(8):573-08.
29. Khosroshahi ME, Ghazanfari L. Synthesis and functionalization of SiO2 coated Fe3O4 nanoparticles with amine groups based on self-assembly. Materials Science and Engineering C: Biomimetic and Supramolecular Systems. 2012;32(5):1043-9.
30. Elliott AM, Shetty AM, Wang J, Hazle JD, Jason Stafford R. Use of gold nanoshells to constrain and enhance laser thermal therapy of metastatic liver tumours. International Journal of Hyperthermia. 2010;26(5):434-40.
31. Loo C, Lowery A, Halas N, West J, Drezek R. Immunotargeted nanoshells for integrated cancer imaging and therapy. Nano letters. 2005;5(4):709-11.
32. Jordan A, Scholz R, Maier-Hauff K, Johannsen M, Wust P, Nadobny J, et al. Presentation of a new magnetic field therapy system for the treatment of human solid tumors with magnetic fluid hyperthermia. J Magn Magn Mater 2001;225(1):118-26.
33. Bulte JWM, Kraitchman DL. Iron oxide MR contrast agents for molecular and cellular imaging. NMR Biomed. 2004;17(7):484-99.
34. Khosroshahi ME, Ghazanfari L. Physicochemical characterization of Fe3O4/SiO2/Au multilayer nanostructure. Mater Chem Phys. 2012;133:55-62.
35. Raschke G, Brogl S, Susha A, Rogach A, Klar T, Feldmann J, et al. Gold nanoshells improve single nanoparticle molecular sensors. Nano letters. 2004;4(10):1853-7.
36. Khosroshahi ME, Nourbakhsh MS, Ghazanfari L. Synthesis and Biomedical Application of SiO2/Au Nanofluid Based on Laser-Induced Surface Plasmon Resonance Thermal Effect. J Modern Phys. 2011;2(9):944-53.
37. Schneider G, Decher G. From functional core/shell nano-particles prepared via layer-by-layer deposition to empty nanospheres. Nano Letters 2004;4:1833-9.
38. Shalaev VM, Kawata S. Nanophotonics with surface plasmons: Elsevier Science; 2007.
39. Duff D, Baiker A, Edwards P. A new hydrogel of gold cluster: formation and particle size variation. Langmuir. 1993;9:2301-9.
40. Vera J, Bayazitoglu Y. Gold nanoshell density variation with laser power for induced hyperthermia. Int J Heat Mass Transfer. 2009;52(3):564-73.
41. O'Neal DP, Hirsch LR, Halas NJ, Payne JD, West JL. Photo-thermal tumor ablation in mice using near infrared-absorbing nanoparticles. Cancer Lett. 2004 Jun 25;209(2):171-6.
42. Kong G, Braun RD, Dewhirst MW. Hyperthermia enables tumor-specific nanoparticle delivery: effect of particle size. Cancer Res. 2000 Aug 15;60(16):4440-5.
43. Maeda H, Fang J, Inutsuka T, Kitamoto Y. Vascular permeability enhancement in solid tumor: various factors, mechanisms involved and its implications. Int Immunopharmacol. 2003 Mar;3(3):319-28.
44. Huang X, Jain PK, El-Sayed IH, El-Sayed MA. Plasmonic photothermal therapy (PPTT) using gold nanoparticles. Lasers Med Sci. 2008 Jul;23(3):217-28.
45. Kah JC, Wan RC, Wong KY, Mhaisalkar S, Sheppard CJ, Olivo M. Combinatorial treatment of photothermal therapy using gold nanoshells with conventional photodynamic therapy to improve treatment efficacy: an in vitro study. Lasers Surg Med. 2008 Oct;40(8):584-9.

46. Nourbakhsh MS, Khosroshahi ME. An in-vitro investigation of skin tissue soldering using gold nanoshells and diode laser. Lasers Med Sci. 2011 Jan;26(1):49-55.
47. Khosroshahi ME, Ghazanfari L. Preparation and characterization of Silica-coated iron-oxide bionanoparticles under N2 gas. Physica E 2010;42:1824-1829.
48. Pham T, Jackson JB, Halas N and Lee TR. Preparation and characterization of gold nano-shells coated with self-assembled monolayers. Langmuir. 2002;18:4915-20.
49. Scholz SM, Vacassy R, Dutta J, Hofmann H, Akinc M. Mie scattering effects from monodispersed ZnS nanospheres. J Appl Phys. 1998;83:7860-6.
50. Joanitti GA, Azevedo RB, Freitas SM. Apoptosis and lysosome membrane permeabilization induction on breast cancer cells by an anticarcinogenic Bowman-Birk protease inhibitor from Vigna unguiculata seeds. Cancer Lett. 2010 Jul 1;293(1):73-81.
51. Hirsch LR, Stafford RJ, Bankson JA, Sershen SR, Rivera B, Price RE, et al. Nanoshell-mediated near-infrared thermal therapy of tumors under magnetic resonance guidance. Proc Natl Acad Sci U S A. 2003 Nov 11;100(23):13549-54.
52. Ntziachristos V, Yodh AG, Schnall M, Chance B. Concurrent MRI and diffuse optical tomography of breast after indocyanine green enhancement. Proc Natl Acad Sci U S A. 2000 Mar 14;97(6):2767-72.
53. Schotter J, Bethge O, Maier T, Brueck H. Recognition of biomolecular interactions by plasmon resonance shifts in single- and multicomponent magnetic nanoparticles. Appl Phys Letters 2008;93:144105-07.
54. Pustovalov V, Astafyeva L, Jean B. Computer modeling of the optical properties and heating of spherical gold and silica-gold nanoparticles for laser combined imaging and photothermal treatment. Nanotechnology. 2009 Jun 3;20(22):225105.
55. Lee YY, Wong KT, Tan J, Toh PC, Mao Y, Brusic V, et al. Overexpression of heat shock proteins (HSPs) in CHO cells for extended culture viability and improved recombinant protein production. J Biotechnol. 2009 Aug 10;143(1):34-43.
56. Nikfarjam M, Muralidharan V, Christophi C. Mechanisms of focal heat destruction of liver tumors. J Surg Res. 2005 Aug;127(2):208-23.
57. Clark AW, Robins HI, Vorpahl JW, Yatvin MB. Structural changes in murine cancer associated with hyperthermia and lidocaine. Cancer Res. 1983 Apr;43(4):1716-23.
58. Soto-Cerrato V, Montaner B, Martinell M, Vilaseca M, Giralt E, Perez-Tomas R. Cell cycle arrest and proapoptotic effects of the anticancer cyclodepsipeptide serratamolide (AT514) are independent of p53 status in breast cancer cells. Biochem Pharmacol. 2005 Dec 19;71(1-2):32-41.
59. Missirlis YF, Spiliotis AD. Assessment of techniques used in calculating cell-material interactions. Biomol Eng. 2002 Aug;19(2-6):287-94.
60. Simhon D, Halpern M, Brosh T, Vasilyev T, Kariv N, Argaman R, et al. A. In vivo laser soldering of incisions in juvenile pig skin, using GaAs or CO2 lasers and a temperature control system. SPIE Proc. 2004; 5312:162-75.